Theoretical Study of the Lowest ^1B_U States of *trans*-Stilbene

Laura Gagliardi,*,† Giorgio Orlandi,*,† Vicent Molina,‡ Per-Åke Malmqvist,‡ and Björn Roos‡

Dipartimento di Chimica G. Ciamician, Università di Bologna, Viale F. Selmi 2, I-40126 Bologna, Italy, and Department of Theoretical Chemistry, Chemical Center, P.O.Box 124, S-221 00 Lund, Sweden

Received: February 11, 2002; In Final Form: May 22, 2002

The results of a theoretical study of the ground state, 1^1A_g, and of the lowest ^1B_u states of *trans*-stilbene are presented. The vertical and adiabatic excitation energies of the lowest ^1B_u states have been computed using multiconfigurational SCF theory, followed by second-order perturbation theory. It is shown that the two lowest excited states are separated by a small energy gap in the Franck−Condon region. They are the 1^1B_u, characterized by the HOMO→LUMO single excitation substantially localized on the ethylenic moiety, and the 2^1B_u, formed by a combination of one electron excitations localized mainly on the benzene rings. The most intense transition is found to be the lowest in energy when the interaction between different states is included at the level of second-order perturbation theory. The vibronic structure of emission and absorption spectra of the two lowest ^1B_u states have been determined within the Franck−Condon approximation. The spectrum calculated for the 1^1B_u state agrees with the experimental spectrum, while the low intensity band computed for the 2^1B_u state has no experimental counterpart. It is concluded that this band is buried in the strong 1^1B_u absorption and therefore not observed.

1. Introduction

Stilbene and stilbene-type molecules have attracted a widespread interest of both theoretical and experimental chemists for more than 60 years because they are prototype molecules for the study of electronic excited state deactivation and of the mechanism of photoreactivity. The modeling of the photoisomerization is easier than other photoprocesses because its reaction coordinate, the torsion around the central CC bond leading to trans−cis isomerization, is well defined. Thus, the trans-cis photoisomerization of stilbene has been extensively studied both experimentally[1−11] and theoretically.[12−16]

According to the commonly accepted picture, the mechanism of cis−trans photoisomerization of *trans*-stilbene (TS) is based on the following concepts:

- The S_1 state, belonging to the B_u representation of the C_{2h} point group, is to a large extent characterized by the HOMO→LUMO excitation. As indicated by quantum yield and lifetime of fluorescence spectra and by intensity of the lowest energy absorption band, it has large transition oscillator strength. Its HOMO→LUMO character leads, as in ethylene, to a flat potential energy surface and this makes isomerization feasible in the S_1 excited state in accordance with the Woodward-Hoffmann rules.[17,18]
- The doubly excited HOMO, HOMO→LUMO, LUMO singlet state, of A_g symmetry, observed in the two-photon spectroscopy, may become the lowest excited state at the twisted geometry and favor the photoisomerization.[19]
- The decay from the S_1 state to the ground state and the photoisomerization process may be enhanced by a conical intersection between S_0 and S_1.[20]

A quantitative assessment of the ordering of the lowest electronic states and of the shapes of their potential energy surfaces and thus of the contributions of these mechanisms to the decay of S_1 is still lacking. An important step in this direction is provided by a recent paper by Molina et al.,[16] in which a quantum chemical study of the vertical transitions of the low-lying excited states of TS, using multiconfigurational wave functions (CASSCF) and second order perturbation theory (CASPT2), is reported. The results of this study were in general in good agreement with experimental data. In particular, they have been useful for the assignment of the two-photon spectra of TS recently investigated by Hohlneicher et al.[11]

However, surprisingly, the electronic state associated to the lowest intense transition, described mainly by a one-electron promotion of HOMO→LUMO type, with an oscillator strength of 0.7 (denoted hereafter as ^1B_u(HL)), was found to correspond to the 2^1B_u state. Its calculated energy, at 4.07 eV, is in good agreement with the experimental measure, which is around 4.0 eV. The 1^1B_u state was found at lower energy, 3.77 eV above the ground state, with an oscillator strength of 0.04. It is of the L_b benzenic type and is described mainly by a combination of the singly excited configurations HOMO→(LUMO+1) and (HOMO-1)→LUMO (denoted hereafter as $^1B_u(-)$).

The prediction of a weak transition ^1B_u below the allowed HOMO→LUMO state is in disagreement with experimental evidence[2−5,11] and also with earlier theoretical studies,[12−15,18] which possibly benefited from errors cancellation. The authors discussed this discrepancy, noting that the amount of the vertical separation between the two lowest ^1B_u states, 0.3 eV, is of the same order of magnitude as the accuracy of the computational methods used.[16] Furthermore, they suggest that the ordering of two states may depend on the molecular geometry and this was proposed also in a recent study by Hohlneicher et al.[11] The issue is of some importance, not only for its implications on the dynamics of the trans−cis photoisomerization process, but also from the methodological point of view, that is with reference to the accuracy and reliability of the CASSCF/CASPT2[21−23] approach in the case of two close-lying electronic states. When

* Corresponding authors. Laura Gagliardi (e-mail: laurag@ciam.unibo.it.). Giorgio Orlandi (e-mail: gorlandi@ciam.unibo.it).
† Dipartimento di Chimica G. Ciamician.
‡ Department of Theoretical Chemistry.

10.1021/jp0256138 CCC: $22.00
Published on Web 07/18/2002

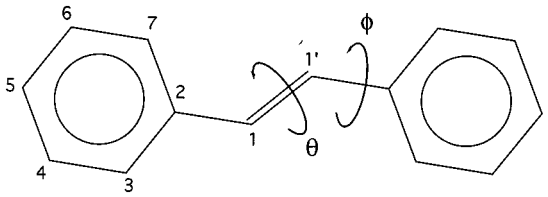

Figure 1. The structure of stilbene, with atoms numbered as in the article.

states are so close as here, this method becomes quite uncertain and the interactions between the states at the correlated level might change their ordering. Recently, in 1998, the CASPT2 method was extended to include such effects.[24] This resulted in the multi-state (MS) CASPT2 approach, which includes the interaction between the different states at the level of second order perturbation theory. It has shown to be able to treat such interactions successfully in a number of applications.

The present work reexamines the ordering of the lowest excited states of TS, using this more advanced technique. We have performed the calculations using an enlarged active space, which includes all 14 π-orbitals with 14 active electrons, while Molina et al.[16] used a 10/12 active space. The typical C=C central bond distance (C_1-C_1 in Figure 1) was optimized pointwise at the MS−CASPT2 level of theory, and for each geometry several ^1B_u excited states were computed.

However, more important for the analysis of the absorption and fluorescence spectra is the possibility we have today of computing not only the vertical excitation energies, but also the geometry of the excited states and harmonic frequencies at the CASSCF level of theory. This gives us the possibility to model the Franck−Condon spectra, which allows a detailed discussion of the character of the two ^1B_u states with respect to their geometry and the shape of the energy surface around the equilibrium geometry. Comparison to the observed spectra becomes more meaningful. One should remember that the vertical excitation energy is a theoretical concept and can be estimated by experiment only qualitatively. With the Franck−Condon spectra available, a direct comparison of the 0−0 transitions and the vibronic progressions becomes possible. We have recently published such an analysis for the two-photon allowed excitation to the ^2A_g state.[25] Here we shall do the same for the two lowest state of ^1B_u symmetry.

2. Computational Details

Complete Active Space (CAS) SCF[21] calculations have been performed and the dynamic electron correlation was added using multiconfigurational second-order perturbation theory, MS−CASPT2.[22−24] The MOLCAS-5 quantum chemistry program[26] was used.

The active space choice is a crucial step in a CASSCF calculation. The stilbene molecule with its 14 valence π MO's and 14 π electrons is a challenging case. In this study, the dependence of the geometry on the active space choice has been investigated for the ground state. We explored several possibilities going from a minimal choice of 10 active electrons in 10 active π MO's (10/10), up to the largest calculation including all the 14 active electrons in the 14 active valence π MO's (14/14). As intermediate cases, we performed the calculation with 10 active electrons in 12 active π MO's (10/12), as already performed by Molina et al.,[16] and 12 active electrons in 12 active orbitals (12/12). All these calculations were performed in C_{2h} symmetry (planar molecule). By placing the molecule in the xy plane, the π orbitals belong to the a_u and b_g irreducible representations of C_{2h}. In the 14/14 calculation, for example, the active space is composed by 0,0,7,7, active orbitals in the four irreducible representations a_g, b_u, a_u, and b_g, respectively.

Generally contracted basis sets of atomic natural orbital (ANO) type were used with the contraction scheme 3s2p1d on C and 2s1p on H.[27] The geometry of the ground state and two excited ^1B_u states were optimized at the CASSCF level by computing analytical first derivatives.[2] The ethylenic C=C bond was reoptimized pointwise at the 14/14 CASPT2 level of theory. The geometry of the ground state was also optimized using density functional theory (DFT), with the B3LYP exchange-correlation functional, and a 6-31G* basis set. The program Gaussian98 was employed.

The 10/12-CASSCF harmonic frequencies (10/12 frequency calculation at the 10/12 optimized geometry) for the 1^1A_g and 1^1B_u states were computed using analytical second derivatives. It was not feasible to perform such calculations using a larger active space.

The multistate option (MS) of the CASPT2 method was used to study the ^1B_u states. This is a new feature of MOLCAS-5 that allows to perform CASPT2 calculations for a number of the selected roots from a state average CASSCF calculation (in this case three B_u states). An effective Hamiltonian constructed by second-order perturbation theory is diagonalized to obtain the final MS−CASPT2 energies.[24]

The method was used to compute excitation energies at the optimized geometries and also at intermediate points where the ethylenic C_1-C_1 distance was varied pointwise together with the ethylene−phenyl (C_1-C_2) distance (see Figure 1 for the numbering of the atoms). CASPT2 calculations were performed for the ground state at the same points. In this way it was possible to study the ordering of the ^1B_u states as a function of the most important geometry parameters. The oscillator strengths have been obtained using the "mixed" reference functions that are obtained from the MS-CASPT2 calculation. To compare our results with the experimental data of Hohlneicher et al.,[11] the vibronic spectra of the two ^1B_u states were computed according to the Franck−Condon mechanism. Harmonic force fields at the equilibrium geometries were computed analytically using the 10/12 CASSCF wave functions. For the B_u states, a common set of force constants was used, obtained from the 10/12 CASSCF wave function. The intensities were estimated from Franck−Condon factors, and a spectrum was constructed from Lorentzian line profiles. The profile of the computed spectrum depends strongly on the amount of displacement of the equilibrium nuclear coordinates along vibration modes and on vibrational frequencies of the final state and therefore gives a sensitive measure of the accuracy of the geometry of the excited state. The calculations of Franck−Condon factors were performed with a recent program, capable of treating states with several excited vibrational quanta in a large number of modes.[29]

3. Results and Discussion

3.1. Geometries and Relative Energies. In Table 1 the ground-state equilibrium geometries obtained at the CASSCF level with different active spaces are presented. The central C_1-C_1 bond length obtained with the 10/12 active space is the same as the 14/14 value, while the 10/10 and 12/12 calculations give a slightly shorter C_1-C_1 bond. The 14/14 CASPT2 C_1-C_1 bond length is 1.363 Å. This value is slightly longer than the 14/14 CASSCF result, and it is also longer than the experimentally accepted value, which is between 1.33 and 1.35 Å.[30−32] The latter value is most likely correct, because this bond should be longer than in ethylene, due to conjugation with the phenyl rings. It appears that CASSCF with all π-orbitals active gives accurate

TABLE 1: Geometry of the 1^1A_g State at the CASSCF Level, with Different Active Spaces[a]

	10/10	10/12	12/12	14/14[b]	B3LYP	exptl[c]
$r(C_1-C_1)$	1.332	1.349	1.329	1.350	1.349	1.326 (1.35−1.36)
$r(C_1-C_2)$	1.473	1.477	1.480	1.476	1.466	1.471
$r(C_2-C_3)$	1.391	1.397	1.402	1.404	1.408	1.392
$r(C_3-C_4)$	1.399	1.399	1.400	1.399	1.393	1.384
$r(C_4-C_5)$	1.392	1.378	1.395	1.396	1.395	1.381
$r(C_5-C_6)$	1.402	1.402	1.402	1.402	1.399	1.383
$R(C_6-C_7)$	1.391	1.389	1.394	1.394	1.391	1.381
$r(C_2-C_7)$	1.406	1.409	1.408	1.409	1.409	1.397
$\angle(C_1C_1C_2)$	126.9	126.6	126.8	126.7	127.2	126.4
$\angle(C_1C_2C_3)$	118.4	118.6	118.4	118.5	118.6	119.0
$\angle(C_1C_2C_7)$	123.5	123.5	123.6	123.6	123.7	123.2
A	2.731	2.733	2.717	2.714	2.715	2.611
B	0.263	0.261	0.261	0.261	0.261	0.263
C	0.240	0.238	0.238	0.238	0.238	0.241

[a] Bond distances in angstroms, and angles in degrees. The rotational constants *A*, *B*, and *C* are in GHz. Comparative DFT/B3LYP results are also reported. [b] **G1** structure. [c] Reference 31.

TABLE 2: 1^1B_u and 2^1B_u Geometry with Different Active Spaces[a]

	10/12[b] 1^1B_u	12/12 1^1B_u	14/14[c] 1^1B_u	14/14[d] 2^1B_u
$r(C_1-C_1)$	1.409	1.342	1.383	1.505
$r(C_1-C_2)$	1.414	1.454	1.435	1.419
$r(C_2-C_3)$	1.439	1.428	1.434	1.443
$r(C_3-C_4)$	1.408	1.415	1.414	1.379
$r(C_4-C_5)$	1.377	1.413	1.410	1.437
$r(C_5-C_6)$	1.413	1.414	1.413	1.428
$r(C_6-C_7)$	1.414	1.417	1.417	1.379
$r(C_2-C_7)$	1.433	1.427	1.430	1.450
$\angle(C_1C_1C_2)$	125.6	126.7	126.5	124.7
$\angle(C_1C_2C_3)$	118.5	118.5	118.6	119.4
$\angle(C_1C_2C_7)$	124.3	123.8	123.9	123.9
A	2.670	2.659	2.653	2.599
B	0.263	0.260	0.260	0.260
C	0.239	0.237	0.237	0.236

[a] Bond distances in angstroms, and angles in degrees. The rotational constants *A*, *B*, and *C* are in GHz. [b] **G3** structure. [c] **G2** structure. [d] **G4** structure.

geometries. Using the CASPT2 approach is not expected to increase the accuracy, unless considerably larger basis sets than those used in this work are employed.

The 10/12 and 14/14 optimizations give the same value for the C_1-C_2 distance, while 10/10 gives a slightly smaller and 12/12 a slightly larger value. All active spaces give the C−C ring distances within the range 1.39−1.40 Å, except for 10/12, which gives an unexpectedly small value of 1.378 Å for the C_4-C_5 bond. This bond is also shorter than other ring bonds in the ^1B_u excited states. The result appears to be an artifact of the 10/12 active space, which gives an unbalanced description of the electronic structure in the phenyl rings.

The results from a DFT/B3LYP optimization with a 6-31G* basis set are also reported in Table 1. We notice the close agreement between these results and those of the 14/14 CASSCF calculation.

The calculated rotational constants suggest a slightly more extended molecular structure than indicated experimentally.

The 1^1B_u equilibrium geometries and rotational constants obtained with three different active spaces are reported in Table 2. The central C_1-C_1 bond varies considerably with the active space. As for the ground state, an accurate description of the geometry requires the 14/14 full π-valence space. The geometry obtained with this active space shows an elongation of the double bond from 1.35 to 1.38 Å and a corresponding shortening of the phenyl bond from 1.47 to 1.44 Å, with respect to the ground state. The changes in the central C−C bonds are rather modest, in agreement with the fact that the $1^1A_g \rightarrow 1^1B_u$ excitation is mainly located in the phenyl rings, at the CASSCF level of theory. It can therefore be related to the $^1B_u(-)$ state. The 10/12 active space assigns a small value of 1.377 Å for the C_4-C_5 bond, as already found for the ground state.

The optimized geometry of 2^1B_u state with the 14/14 active space shows a longer central C_1-C_1 bond, 1.505 Å, and a shorter C_1-C_2 bond, 1.419 Å. Clearly the excitation to this state affects substantially the central moiety of TS.

The analysis of the 14/14 wave function of the 1^1B_u state at its equilibrium geometry shows that this state has a strong multiconfigurational character, with a small weight of the HOMO→LUMO configuration and a modest oscillator strength (<0.05). This state does not correspond to the ionic ^1B_u state responsible for the lowest, strong band in the absorption spectrum. Actually, as we shall see below, the state dominated by the HOMO→LUMO configuration, with large oscillator strength, is the second at this optimized geometry.

With the 10/12 active space, the wave function of the 1^1B_u state at the optimized geometry shows a larger HOMO→LUMO character and a sizable oscillator strength (ca. 0.3). This state thus resembles more the B_u(HL) state, which is the lowest by experiment. Clearly, the ordering of the three close lying excited states depends on the molecular geometry, on the active space used, and on the amount of correlation included. The reordering of the different states for different geometries makes it very difficult to optimize the geometry of the HOMO→LUMO state with the 14/14 active space.

Therefore, we decided to perform single point calculations at the (state average) CASSCF, CASPT2, and MS-CASPT2 levels of theory for the three lowest B_u states with a 14/14 active space at the following CASSCF optimized geometries (angstrom):

		$R(C_1-C_1)$	$R(C_1-C_2)$
geometry			
1^1A_g(14/14)	**G1**	1.350	1.476
1^1B_u(14/14)	**G2**	1.383	1.435
1^1B_u(10/12)	**G3**	1.409	1.414
intermediate geometry	**G34**	1.441	1.414
2^1B_u(14/14)	**G4**	1.505	1.419

The geometries are those reported in Table 1 (**G1**), and Table 2 (**G2**, **G3**, and **G4**). One additional intermediate geometry was added to the list of optimized geometries, (**G34**), in which the geometric parameters for the central moiety were taken from an average of **G3** and **G4** geometries while the ring structure was taken from **G4** geometry. We have then constructed the potential energy curves for the three lowest ^1B_u states as a function of the C_1-C_1' bond distance.

TABLE 3: Adiabatic Energy Differences (eV) with Respect to 1^1A_g State, and Oscillator Strength for the Three B_u States at Various Geometries

geometry	G1	G2	G3	G34	G4
$r(C_1-C_1)$	1.350	1.383	1.409	1.441	1.505
$r(C_1-C_2)$	1.476	1.435	1.414	1.414	1.418
CASSCF	4.80 (0.01)	4.70 (0.01)	4.70 (0.01)	4.73 (0.65)	4.99 (1.01)
	6.26 (1.25)	6.05 (1.12)	5.97 (1.32)	5.89 (0.45)	5.55 (0.01)
	6.41 (0.02)	6.14 (0.23)	6.06 (0.22)	6.08 (0.05)	6.26 (0.01)
CASPT2	4.03 (0.01)	3.84 (0.01)	3.83 (0.01)	3.77 (0.51)	3.70 (1.05)
	4.04 (0.81)	4.00 (0.74)	4.00 (0.88)	3.85 (0.29)	4.11 (0.01)
	5.70 (0.02)	5.11 (0.19)	4.91 (0.18)	5.17 (0.04)	4.93 (0.01)
MS-PT2	3.86 (0.49)	3.40 (0.68)	3.30 (0.60)	3.52 (0.49)	3.61 (0.73)
	4.17 (0.32)	3.93 (0.09)	3.91 (0.01)	3.97 (0.28)	4.17 (0.01)
	5.73 (0.01)	5.63 (0.01)	5.53 (0.22)	5.30 (0.05)	4.96 (0.01)

TABLE 4: MS-CASPT2 Mixing at the Various Geometries of the Three Lowest ^1B_u States

geometry	S_1 CASPT2	S_2 CASPT2	S_3 CASPT2
G1			
S_1 MSPT2	0.68	−0.73	−0.02
S_2 MSPT2	0.73	0.67	0.14
S_3 MSPT2	−0.09	−0.11	0.99
G2			
S_1 MSPT2	0.41	−0.91	0.01
S_2 MSPT2	0.80	0.35	−0.49
S_3 MSPT2	0.44	0.21	0.87
G3			
S_1 MSPT2	0.37	−0.93	−0.00
S_2 MSPT2	0.78	0.31	0.54
S_3 MSPT2	0.50	−0.20	0.84
G34			
S_1 MSPT2	0.83	−0.49	0.28
S_2 MSPT2	0.51	0.86	−0.00
S_3 MSPT2	−0.24	0.15	0.96
G4			
S_1 MSPT2	0.94	0.32	0.15
S_2 MSPT2	−0.32	0.95	−0.00
S_3 MSPT2	−0.15	−0.05	0.99

The energy differences of the three ^1B_u states at the above 5 different geometries with respect to the 1^1A_g state at its **G1** equilibrium geometry are reported in Table 3 together with oscillator strengths. A striking result is the dependence of the state ordering on the level of theory.

At the CASPT2 level, the $^1B_u(-)$ state is found to be the lowest state for the **G1**, **G2**, and **G3** geometries, while at the **G4** geometry the ^1B_u(HL) state is lower. The lowest state at the intermediate **G34** geometry, has contributions from both types of excitations although the ^1B_u(HL) character dominates. The result shows that a correct description of the S_1 state is only obtained when the interaction between the lowest states is included at the correlated level The contributions from the different CASSCF states to the wave functions at the MS-CASPT2 level is shown in Table 4.

The table gives the weight of the different CASPT2 wave functions for the three MS-CASPT2 states at different geometries. For all geometries there is a considerable mixing of the two lowest states and in all cases will the HOMO→LUMO configuration dominate the lowest excited state. When two, or more, excited states of the same symmetry are close in energy, independent CASPT2 calculations for each of them may not be adequate. It is advisable to allow the states to interact at the correlated level, as is done in the MS-CASPT2 approach.

The computed vertical excitation energies (oscillator strength) for the three ^1B_u states are 4.03 (0.01), 4.04 (0.81), and 5.70 (0.02) at the CASPT2 level, and become 3.86 (0.50), 4.17 (0.32), and 5.73 (0.005) at the MS−CASPT2 level. In the next section we shall discuss the vibrational structure for the emission and absorption spectra of the two lowest ^1B_u states, to show that their different character is reflected also in the Franck−Condon envelop of the two electronic transitions. Here we only notice that the vertical energy for the S_1 has been experimentally found to lie in the energy range 4.0−4.2 eV.[2]

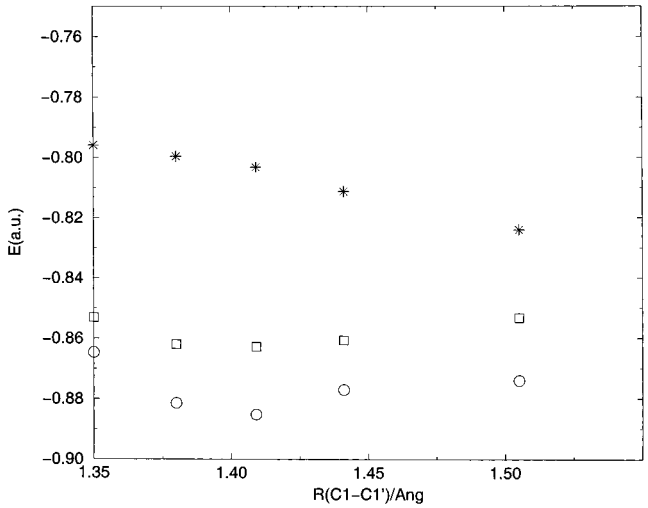

Figure 2. Total energy as a function of the C1−C1 distance for S_1 (solid line), S_2 (dashed), and S_3 states (dotted).

The MS−CASPT2 energy curves of the three ^1B_u states as a function of the C_1-C_1 distance are shown in Figure 2. The intense state is always the lowest and its minimum energy is found for R (C_1-C_1) equal to ca. 1.41 Å, which is a geometry close to **G3**. We see a clear difference between this state and the weakly allowed state. In the strongly allowed state the elongation of the CC double bond is more pronounced, from 1.35 to 1.41 Å, while the phenyl bond has shortened from 1.47 to 1.41 Å. The excitation in the intense ^1B_u state is largely localized in the ethylene fragment. As a consequence we decided to use the **G3** equilibrium geometry in the calculation of the Franck−Condon structure. The result of that calculation provides further evidence that the **G3** geometry corresponds well to the geometry of the strong ^1B_u state (see below).

The computed adiabatic excitation energies for the lowest ^1B_u state is 3.30 eV. This value is lower than the experimental value around 3.8 eV.[11] Thus, the MS-CASPT2 treatment appears to overestimate the interaction between the three states.

3.2. Vibrationally Resolved Absorption and Fluorescence Spectra for the ^1B_u(HL) and $^1B_u(-)$ States. The 10/12 harmonic frequencies for the 1^1A_g and 1^1B_u states, with their assignments, are presented in Tables 5−8. The corresponding force field has been used for the calculation of the vibrationally resolved electronic spectra. The CASSCF frequencies are overall ca. 10% higher than the experimental frequencies. This is due to the use of a harmonic force field, but also to the missing correlation effects in the CASSCF approach. At the CASSCF level, analytic force constants are troublesome when the investigated state interacts with other states. This seems to happen here for the ^1B_u state, where at least some vibrational modes of b_u symmetry are affected (see for example the harmonic frequency of ν_{55}, which is 2490 cm^{-1}). The large IR intensities computed for some vibrational modes also suggest some nonphysical interactions with nearby states, because they typically give large dipole moment derivatives.

The assignment of the lower frequencies out of plane modes (b_g, a_u) for the ground state was taken from our previous study.[33] The calculated vibrational frequencies of the ^1B_u states can be a guideline for the assignment of high-resolution absorption and emission spectra.

TABLE 5: a_g Harmonic Frequencies for the 1^1A_g and 1^1B_u States in cm^{-1}, with the 10/12 Active Space[a]

mode	1^1A_g	exptl[b]	1^1B_u	exptl[b]	assignment
25	215	204	209	198	C_e=C_e−C_{ph} def[c]
24	300	290	284	280	C_e−C_{ph}−C def
23	665	624	625	591	ring def
22	688	646	650	622	ring def
21	919	870	906	849	ring def + C_e=C_e−C_{ph} def
20	1065	1006	1020	995	trigonal+breathing
19	1105	1026	1055	973	CH def+ring def
18	1158	1072	1114	1070	CH def
17	1211	1162	1231		CH def
16	1272	1188	1239		CH def
15	1285	1208	1267	1170	C_e−C_{ph} stretch
14	1339	1315	1536	1249	ring str +CH def
13	1425	1321	1290	1332	C_e=C_e
12	1457	1340	1426	1430	ring stretch + CH def
11	1567	1445	1515	1464	ring stretch
10	1629	1495	1575		ring stretch
9	1718	1584	1631	1530	ring stretch
8	1748	1642	1675	1548	C−C
7	1790	1654	1611	1554	C_e=C_e, C_e−C_{ph}

[a] CH stretches are omitted. [b] Reference 5. [c] def = deformation.

TABLE 6: a_u Harmonic Frequencies for the 1^1A_g and 1^1B_u States, in cm^{-1}, with the 10/12 Active Space[a]

mode	1^1A_g	exptl[b]	1^1B_u	exptl[c]	assignment[d]
37	-i10 (0.0)		54 (0.0)	47.5	Ce−C_{ph} tors
36	60 (0.3)		248 (0.3)	276	Ce−C_{ph} flap
35	299 (0.0)	275	50 (0.2)	35	Ce=Ce tors, ring def
34	433 (0.0)	403	370 (0.8)	358	ring tors
33	559 (18.9)	528	517 (20.5)	418	Ce=Ce tors, ring def
32	735 (54.0)	693	651 (70.4)		ring def
31	807 (123)	764	707 (55.9)		CH wag
30	883 (8.2)	848	773 (65.3)		CH wag
29	957 (0.3)	909	889(47.4)		C_eH def
28	1009 (35.9)	966	833 (7.8)		CH wag
27	1022 (2.8)	972	925 (2.2)		CH wag
26	1082 (0.0)	985	1043 (0.0)		CH wag

[a] IR intensities within parantheses. [b] Reference 34. [c] References 35−39. [d] tors = torsional, def = deformation, wag = wagging.

TABLE 7: b_g Harmonic Frequencies for the 1^1A_g and 1^1B_u States, in cm^{-1}, with the 10/12 Active Space[a]

mode	1^1A_g	exptl[b]	1^1B_u	exptl[c]	assignment[d]
48	48	132	129		C_e−C_{ph} wag
47	223	239	301	248	C_e−C_{ph} tors
46	434	410	385	331	ring def
45	495	465	485	410	ring def
44	724	612[e]	643		ring def
43	774	735	704		CH wag
42	836	842	813		CH wag
41	885	916	758		CH wag
40	959	969			C_eH wag
39	1022	969			CH wag
38	1083	985			CH wag

[a] IR intensities within parantheses. [b] Reference 34. [c] References 35−39. [d] tors = torsional, def = deformation, wag = wagging. [e] Reference 40.

Franck−Condon factors that modulate the vibrational structure of electronic transitions depend heavily on the difference between the equilibrium geometries of the initial and final electronic states. Computed absorption spectrum of the ^1B_u(HL) → 1^1A_g transition is shown in Figure 3. All computed spectra have been broadened with Lorenzian line shapes with fwhm = 2 meV (sharp lines) and 50 meV (broad peaks) to simplify comparison with experiment. The experimental spectrum (dashed curve) of Hohlneicher et al.[11] has been inserted. The close resemblance agrees with the notion that the excited-state

TABLE 8: b_u Harmonic Frequencies for the 1^1A_g and 1^1B_u States, in cm^{-1}, with the 10/12 Active (CH Stretches Omitted)[a]

mode	1^1A_g	exptl[a]	1^1B_u	assignment
72	86 (0.2)		87 (0.10)	CCC
71	494 (0.8)	495	502 (4.90)	CCC
70	578 (9.6)	542	536 (30.4)	CCC
69	668 (0.2)	621	620 (46.9)	CCC
68	869 (0.1)	840	892 (27.6)	CCC
67	1064 (0.6)	998	986 (45.8)	CC
66	1105 (4.2)	1032	1038 (7.54)	CCH
65	1158 (6.1)	1072	1115 (3.72)	CCH
64	1206 (3.2)	1157	1132 (159.0)	CCH
63	1271 (0.2)	1172	1252 (4.89)	CCH
62	1313 (0.6)	1216	1328 (62.7)	CC
61	1329 (0.1)	1266	1400 (38.9)	C_{ph}C
60	1414 (3.5)	1303	1462 (13.8)	CC_eH
59	1466 (1.1)	1329	1515 (60.5)	CCH
58	1577 (15.4)	1453	1540 (223.0)	CC,CCH
57	1636 (22.9)	1497	1574 (16.5)	CC,CCH
56	1730 (5.8)	1581	1690 (2.55)	CC
55	1752 (22.4)	1602	2490 (805.0)	CC

[a] IR intensities within parantheses. [b] Reference 34. [c] References 34−38.

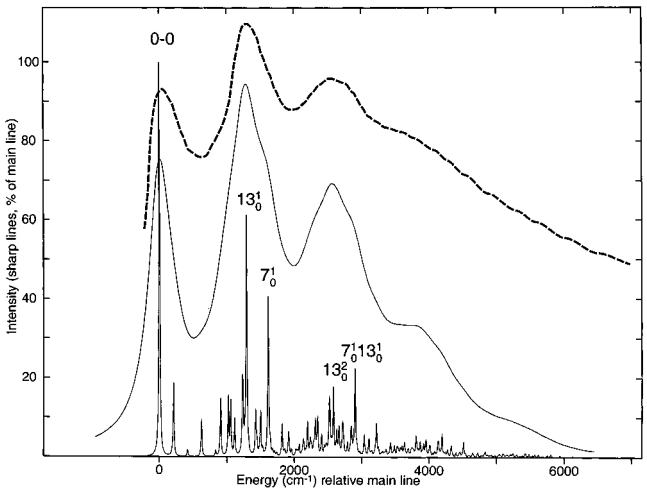

Figure 3. Approximate Franck−Condon intensities for the absorption 1^1A_g→1^1B_u spectrum, assuming a geometry close to the **G3** one (See text). The experimental curve A of ref 11 is also shown (dashed).

responsible for the strong band has an equilibrium geometry close to **G3**. The ν_7 and ν_{13} modes, showing the largest progressions, correspond to structures undergoing large displacements in the transition.

We computed the absorption spectrum also for the weak 2^1B_u state, which has its equilibrium geometry close to **G2**. The calculated spectrum is reported in Figure 4. It is very weak and shows no resemblance to the observed absorption spectrum. Because it is hidden under the stronger absorption of the 1^1B_u state, it will be very difficult to observe.

In a similar way we calculated the vibrational envelope of the fluorescence spectra from the two ^1B_u states. The vibronic structure is governed in both spectra by the normal modes of the ground state.

The calculated emission spectra are shown in Figures 5 and 6.

Assignments of the most prominent features in the fluorescence spectrum for the 1^1B_u(HL) state are given in Table 9. In this Table a comparison is made to the assignments of the bands in the dispersed fluorescence spectrum of Syage et al.[5] From this comparison, the experimental spectrum agrees with the assumption that the geometry of the strong HL state is close to

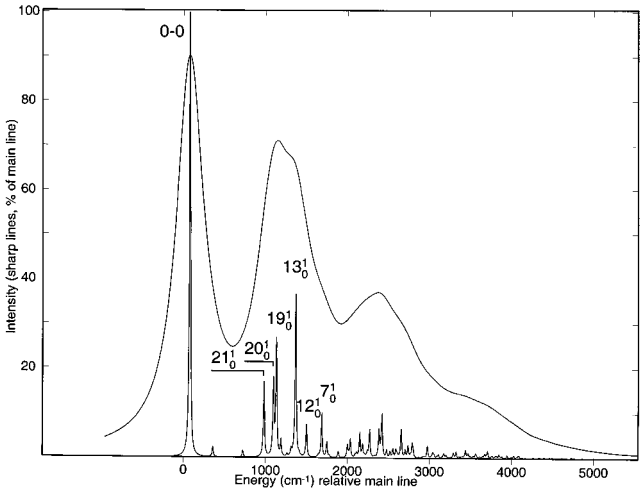

Figure 4. Approximate Franck−Condon intensities for the absorption $1^1A_g \rightarrow 2^1B_u$ spectrum, assuming a geometry close to the **G2** one (See text).

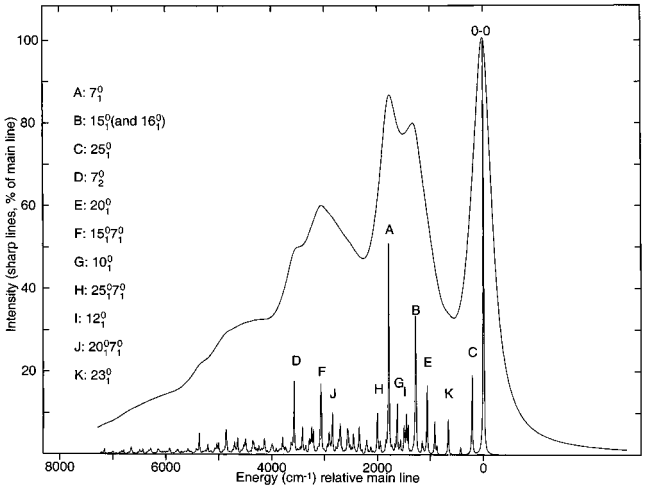

Figure 5. Approximate Franck−Condon intensities for the emission $1^1B_u \rightarrow 1^1A_g$ spectrum.

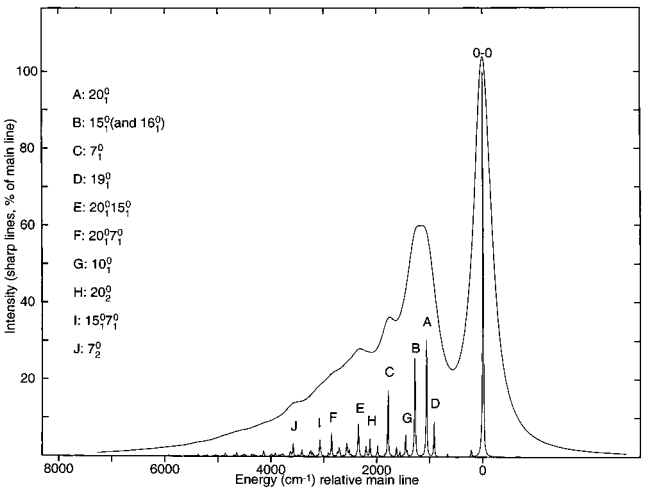

Figure 6. Approximate Franck−Condon intensities for the emission $2^1B_u \rightarrow 1^1A_g$ spectrum.

G3. Comparing the absorption and emission spectra from this state (Figures 3 and 5) shows strong similarities, but also some differences. The ethylenic mode ν_7 gives rise to strong bands in both spectra, while ν_{13} and ν_{15} (both CC stretch) are strong in absorption and emission, respectively (see Table 3 for the definitions of the different a_g modes). These features are also confirmed experimentally (cf. Table 9), which gives 7(0,1) as a strong band at 1654 cm^{-1}. Band 15(0,1) appears as a strong feature at 1208 cm^{-1} experimentally, and at 1286 cm^{-1} in the theoretical spectrum. However, the activity of ν_{25}, (204 cm^{-1}), the CCC bending localized in the ethylene moiety, is not well predicted. In the dispersed fluorescence spectrum the fundamental of ν_{25} has a relative intensity of 71% of the 0−0 band and generates a progression comprising a number of overtones with significant intensity. The computed activity is much lower: the intensity of the fundamental is only 19% of the 0−0 band. According to the Franck−Condon analysis performed by Syage et al.[5] the intensity distribution in this mode is accounted for by a difference of 1.3 ± 0.3 degrees of the bending angle $C_1C_2C_3$ (cf. Figure 1) between S_0 and S_1. The difference between the calculated and observed activity of ν_{25} can be understood considering that the computed $C_1C_2C_3$ angle, (118.5°), is the same in S_0 and S_1.

TABLE 9: Assignments of the Emission Spectrum (cm^{-1}) for the ^1B_u (HL) State[a]

band	this work	exptl[5]
25 (0,1)	215 (19)	204 (71)
25 (0,2)	430 (1.7)	413 (28)
23 (0,1)	665 (8.5)	624 (11)
25 (0,1) 23 (0,1)	880 (1.9)	822 (5.9)
21 (0,1)	919 (7.9)	870 (5.7)
20 (0,1)	1065 (17)	1006 (11)
25 (0,1) 21 (0,1)	1134 (1.4)	1087 (2.5)[b]
18 (0,1)	1158 (2.7)	1072 (3.8)
16 (0,1)	1272 (10.7)	1188 (4.2)
25 (0,1) 20 (0,1)	1279 (2.9)	
15 (0,1)	1286 (28.9)	1208 (13)
13 (0,1)	1425 (6.4)	1321 (5.1) or 1340 (6.8)
12 (0,1)	1457 (9.0)	1340 (6.8)
25 (0,1) 16 (0,1)	1487 (1.9)	1396 (3.5) or 1359 (4.2)
25 (0,1) 15 (0,1)	1500 (5.7)	1413 (5.6)
11 (0,1)	1567 (3.0)	1435 (3.8)[b]
10 (0,1)	1630 (11.2)	1495 (2.8)
25 (0,1) 13 (0,1)	1640 (1.8)	
25 (0,1) 12 (0,1)	1672 (1.8)	1541 (4.3)
23 (0,1) 20 (0,1)	1729 (1.3)	
7 (0,1)	1790 (50.5)	1654 (20)
25 (0,1) 10 (0,1)	1844 (2.2)	1698 (2.3)[c]
23 (0,1) 15 (0,1)	1950 (2.4)	1822 (5.5)[c]
21 (0,1) 20 (0,1)	1984 (1.3)	
25 (0,1) 7 (0,1)	2005 (9.7)	1855 (13)
20 (0,2)	2129 (1.3)	
21 (0,1) 15 (0,1)	2205 (2.6)	2063 (5.4)[b]
20 (0,1) 16 (0,1)	2337 (2.0)	
20 (0,1) 15 (0,1)	2350 (5.3)	
23 (0,1) 7 (0,1)	2455 (4.5)	

[a] Comparison to the work by Syage et al. ref 5. IR intensities within parantheses. [b] New assignment. [c] Alternative assignment.

Table 9 lists only bands below 2500 cm^{-1} with a relative intensity larger than 1. The computed spectrum does not correspond strictly in all the details to the observed spectrum by Syage et al.[5] because of the limited accuracy of the computed vibrational force fields of the S_0 and S_1 states.

If we disregard the fine details and model the spectrum at lower resolution, by broadening the line width of each band, we get better agreement between theory and experiment. This indicates that the calculation reproduces the main features of the geometry changes in the S_0-S_1 transition and the overall shape of the spectra.

4. Conclusions

We have presented the results of a study of the 1^1A_g ground state and the two lowest excited states of ^1B_u symmetry for

trans-stilbene. A weak state of the same symmetry was found in the vicinity of the well-known HOMO→LUMO ^1B_u state. The ordering of the two states has been shown to depend strongly on the level of approximation used in the calculations. Only at the MS−CASPT2 level of theory was the intense state found to be lower in energy. The vibronically resolved absorption and fluorescence spectra of the two states have been determined within the Franck−Condon approximation. The computed vibronic intensity distribution for the 1^1B_u state is in close agreement with experiment, which confirms that the computed equilibrium geometry for this state is correct. The weak state gives rise to a completely different vibronic structure. The corresponding absorption band is hidden under the 1^1B_u (HL) band and will be difficult to observe.

Acknowledgment. This work was partially supported by Ministero dell'Università e della Ricerca Scientifica (Project: Modellistica delle Proprieta' Spettroscopiche di Sistemi Molecolari Complessi, funds ex 60%. Project: Dinamiche Molecolari in Sistemi di Interesse Chimico, funds ex 40%), the Swedish Natural Science Research council, and by the EU Research and Training Network THEONET-II (Contract HPRN-CT-1999-00005). V.M. thanks a postdoctoral fellowship from the MEC of Spain.

References and Notes

(1) Malkin, S.; Fischer, E. *J. Phys. Chem.* **1964**, *68*, 1153.

(2) Saltiel, J.; D'Agostino, J.; Megarity, D. E.; Metts, L.; Neuberger, K. R.; Wrighton, M.; Zafarion, O. C. *Org. Photochem.* **1971**, *3*, 1. Saltiel, J.; Sun, Y.-P. In *Photochromism Molecules and Systems*; Durr, H., Bouas-Laurent, H., Eds.; Elsevier: New York, 1990; p 64. Saltiel, J.; Sun, Y.-P. *J. Phys. Chem.* **1989**, *93*, 8310.

(3) Hochstrasser, R. M. *Pure Applied Chemistry* **1980**, *52*, 2683. Sension, R. S.; Repinec, S. T.; Szarka, A. Z.; Hochstrasser, R. M. *J. Chem. Phys.* **1993**, *98*, 6291. Champagne, B. B.; Pfansfiel, J. P.; Plusquellic, D. F.; Pratt, D. W.; van Harpen, W. M.; Meerts, W. L. *J. Phys. Chem.* **1990**, *94*, 6.

(4) Waldeck, D. H. *Chem. Rev.* **1991**, *91*, 415.

(5) Syage, J. A.; Felker, P. M.; Zewail, A. H. L. *Chem. Phys.* **1981**, *11*, 4685; Syage, J. A.; Lambert, W. R.; Felker, P. M.; Zewail, A. H.; Hochstrasser, R. M. *Chem. Phys. Lett.* **1982**, *88*, 266. Syage, J. A.; Felker, P. M.; Zewail, A. H. *J. Chem. Phys.* **1984**, *81*, 4706. Felker, P. M.; Zewail, A. H. *J. Phys. Chem.* **1985**, *89*, 5402.

(6) Meier, H. *Angew. Chem.* **1992**, *31*, 1399.

(7) Arai, T.; Tokumaru, K. *Chem. Rev.* **1993**, *93*, 23. Whitten, D. G. *Acc. Chem. Res.* **1993**, *26*, 502.

(8) Todd, D. C.; Fleming, G. R.; Jean, J. M. *J. Chem. Phys.* **1992**, *97*, 8915.

(9) Goerner, H.; Kuhn, H. J. *Adv. Photochem.* **1995**, *19*, 1.

(10) Gudipati, M. S.; Maus, M.; Daverkausen, J.; Hohlneicher, G. *Chem. Phys.* **1995**, *192*, 37. Hohlneicher, G.; Dick, B. *J. Photochem.* **1984**, *27*, 215.

(11) Hohlneicher, G.; Wrzal, R.; Lenoir, D.; Frank, R. *J. Phys. Chem. A* **1999**, *103*, 8969.

(12) Lhost, O.; Brédas, J. L. *J. Chem. Phys.* **1992**, *96*, 5279.

(13) Arenas, J. F.; López-Tocón, I.; Otero, J. C.; Marcos, J. I. *J. Phys. Chem.* **1992**, *96*, 5279.

(14) Negri, F.; Orlandi, G.; Zerbetto, F. *J. Phys. Chem.* **1989**, *93*, 5124.

(15) Negri, F.; Orlandi, G.; Zerbetto, F. *J. Phys. Chem.* **1994**, *98*, 2254.

(16) Molina, V.; Merchán, M.; Roos, B. O. *J. Phys. Chem. A* **1997**, *101*, 3478.

(17) Woodward, R. B.; Hoffmann, R. *Angew. Chem., Int. Ed. Engl.* **1969**, *8*, 781.

(18) Michl, J.; Bonacic-Koutecky V. *Electronic Aspects of Organic Photochemistry*; Wiley-Interscience: New York, 1990.

(19) Orlandi, G.; Siebrand, W. *Chem. Phys. Lett.* **1975**, *30*, 352.

(20) Bernardi, F.; Olivucci, M.; Robb, M. A. *Chem. Soc. Rev.* **1996**, *25*, 321.

(21) Roos, B. O. In *Advances in Chemical Physics; Ab Initio Methods in Quantum Chemistry−II*; Lawley, K. P., Ed.; John Wiley & Sons Ltd.: Chichester, England, 1987; Chapter 69, p 399.

(22) Andersson, K.; Malmqvist, P.-Å.; Roos, B. O. *J. Chem. Phys.* **1992**, *96*, 1218.

(23) Andersson, K.; Roos, B. O. In Modern Electron Structure Theory. Yarkony, R., Ed.; *Advanced Series in Physical Chemistry*; World Scientific Publishing Co. Pte. Ltd.: Singapore, 1995; Vol. 2, Part I:55.

(24) Finley, J.; Malmqvist, P.-Å.; Roos, B. O.; Serrano-Andrés, L. *Chem. Phys. Lett.* **1998**, *288*, 299−306.

(25) Starling, J.; Gagliardi, L.; Malmqvist, P-Å; Lindh, R. *Mol. Phys.* **2002**, *100*, 1791.

(26) Andersson, K.; Bernhardsson, A.; Blomberg, M. R. A.; Boussard, P.; Cooper, D. L.; Fleig, T.; Fülscher, M. P.; Karlström, G.; Lindh, R.; Malmqvist, P.-Å.; Neogrády, P.; Olsen, J.; Roos, B. O.; Sadlej, A. J.; Schimmelpfennig, B.; Schütz, M.; Seijo, L.; Serrano-Andrés, L.; Siegbahn, P. E. M.; Stålring, J.; Thorsteinsson, T.; Veryazov, V.; Wahlgren, U.; Widmark, P.-O. MOLCAS, version 5.0; Department of Theorerical Chemistry, Chemistry Center, University of Lund: P. O. B. 124, S-221 00 Lund, Sweden, 2000.

(27) Pierloot, K.; Dumez, B.; Widmark, P.-O.; Roos, B. O. *Theor. Chim. Acta* **1995**, *90*, 87.

(28) Lindh, R. *Theor. Chim. Acta* **1993**, *85*, 423.

(29) Bernhardsson, A.; Forsberg, N.; Malmqvist, P.-Å.; Roos, B. O.; Serrano-Andrés, L. *J. Chem. Phys.* **2000**, *112*, 2798−2809.

(30) Traetteberg, M.; Frantsen, E. B.; Mijhoff, F. C.; Hoekstra, A. *J. Mol. Struct.* **1975**, *26*, 57.

(31) Bouwstra, J. A.; Schouten, A.; Kroon, J. *Acta Crystallogr.* **1984**, *C40*, 428.

(32) Ogawa, K.; Harada, J.; Tomoda, S. *Acta Crystallogr.* **1995**, *B51*, 240.

(33) Orlandi, G.; Gagliardi, L.; Melandri, S.; Caminati, W. *J. Mol. Struct.* **2002**, *612*, 383.

(34) Palmo, K. *Spectrochim. Acta* **1988**, *44 A*, 341.

(35) Bree, A.; Edelman, M. *Chem. Phys.* **1980**, *51*, 77.

(36) Meic, Z.; Baranovic, G.; Skare, D. *J. Mol. Struct.* **1986**, *141*, 375.

(37) Suzuki, T.; Mikami, N.; Ito, M. *J. Phys. Chem.* **1987**, *91*, 517.

(38) Urano, T.; Hamaguchi, H.; Tasumi, M.; Yamanouchi, K.; Tsuchiya, S.; Gustafson, T. L. *J. Chem. Phys.* **1989**, *91*, 3884.

(39) Baranovic, G.; Meic, Z.; Gusten, H.; Mink, H.; Keresztury, G. *J. Phys. Chem.* **1990**, *94*, 2833.

(40) Meic, Z.; Gusten, H. *Spectrochim. Acta* **1978**, *34 A*, 101.